Published in final edited form as:
J Neurosci Methods. 2016 July 15; 267: 141–149. doi:10.1016/j.jneumeth.2016.04.012.

Intact skull chronic windows for mesoscopic wide-field imaging in awake mice

Gergely Silasi[1,3], **Dongsheng Xiao**[1,2,3], **Matthieu P. Vanni**[1], **Andrew C. N. Chen**[1,2,*], and **Timothy H. Murphy**[1,*]

[1]Department of Psychiatry, University of British Columbia, Vancouver, BC, Canada

[2]Beijing Institute for Brain Disorders, Capital Medical University, Beijing, China

Abstract

Background—Craniotomy-based window implants are commonly used for microscopic imaging, in head-fixed rodents, however their field of view is typically small and incompatible with mesoscopic functional mapping of cortex.

New Method—We describe a reproducible and simple procedure for chronic through-bone wide-field imaging in awake head-fixed mice providing stable optical access for chronic imaging over large areas of the cortex for months.

Results—The preparation is produced by applying clear-drying dental cement to the intact mouse skull, followed by a glass coverslip to create a partially transparent imaging surface. Surgery time takes about 30 minutes. A single set-screw provides a stable means of attachment for mesoscale assessment without obscuring the cortical field of view.

Comparison with Existing Methods—We demonstrate the utility of this method by showing seed-pixel functional connectivity maps generated from spontaneous cortical activity of GCAMP6 signals in both awake and anesthetized mice.

Conclusions—We propose that the intact skull preparation described here may be used for most longitudinal studies that do not require micron scale resolution and where cortical neural or vascular signals are recorded with intrinsic sensors.

Keywords

Optogenetics; GCaMP; Head-fixed

1. Introduction

The current generation of optogenetic tools provides unprecedented possibilities for selectively mapping and manipulating network elements within the rodent brain (Emiliani et al., 2015). As a result, these methods are growing in popularity for studying the relationship between neuronal activity and behavior in awake mice. Two approaches for delivering light

*Co-corresponding authors. Correspondence should be addressed to A.C. (ac@ccmu.edu.cn) or T.M. (thmurphy@mail.ubc.ca).
[3]Authors contributed equally

to the brain are to either implant a light fiber, or to create a cranial window that provides optical access to the underlying cortex. The fiber-based approach can target subcortical structures that are not accessible via cranial windows (Aravanis et al., 2007; Gaffield et al., 2015), and can sample a field of view as large as 2 mm with the use of head-mounted microendoscopes (Jennings et al., 2015). However, mesoscopic mapping of cortical function– a spatial scale where the relationship among several functional regions can be examined (Oh et al., 2014; Silasi and Murphy, 2014) – requires optical access to an even larger area, with preferably non-invasive preparations to resolve map-like activity.

Cranial windows, such as those developed for chronic 2-photon microscopic imaging, were initially applied in optogenetic studies (Dombeck et al., 2007; Holtmaat et al., 2009), however, the relatively small field of view limits their application in mesoscopic brain mapping, and the invasiveness of the preparation also produces inadvertent brain damage and inflammation (Yang et al., 2010). Several research groups began to take advantage of the semi-transparent nature of the mouse skull by generating large, bi-hemispheric windows through either the intact (Guo et al., 2014), or partially thinned skull (Silasi et al., 2013). Although retraction of the skin alone can have some unwanted effects, such as significant brain cooling in anesthetized mice (Kalmbach and Waters, 2012), the reduced invasiveness offered by transcranial windows has made this the preparation of choice in a number of imaging applications (Cang et al., 2005; Yang et al., 2010; Yoder and Kleinfeld, 2002) including wide-field imaging of hemodynamic signals in anesthetized preparations (Kalchenko et al., 2014; White et al., 2011), and targeted photostimulation in awake (Hira et al., 2009) or behaving mice (Hira et al., 2015). So far, however there have been no detailed methodological descriptions for these preparations, nor has this technique been applied for chronic, wide-field functional imaging in awake mice.

Here we describe a chronic transcranial window preparation that we have previously used for anesthetized imaging (Vanni and Murphy, 2014), and demonstrate its feasibility and stability for bi-hemsipheric wide-field imaging of spontaneous activity in awake mice. Importantly, seed pixel functional connectivity (correlation) maps generated from spontaneous activity in awake mice show similar patterns of connectivity to the anesthetized state, indicating that our preparation facilitates functional cortical mesoscopic mapping in different brain states.

2. Method

2.1. Animals

All procedures were approved by the University of British Columbia Animal Care Committee and conformed to the Canadian Council on Animal Care and Use guidelines. Transgenic GCaMP6s mice (n=11) were produced by crossing Emx1-cre (B6.129S2-Emx1$^{tm1(cre)Krj}$/J, Jax #005628), CaMK2-tTA (B6.Cg-Tg(Camk2a-tTA)1Mmay/DboJ, Jax #007004) and either TITL-GCaMP6s (Ai94; B6.Cg-Igs7$^{tm94.1(tetO\text{-}GCaMP6s)Hze}$/J, Jax #024104) or TITL-GCaMP6f (Ai93; B6.Cg-Igs7$^{tm93.1(tetO\text{-}GCaMP6f)Hze}$/J, Jax #024103) strains (Madisen et al., 2012). The presence of GCaMP expression was determined by genotyping each animal with PCR amplification. This crossing is expected to produce stable expression of GCaMP6 specifically within all excitatory neurons across all layers of the

cortex (Vanni and Murphy, 2014). Control experiments, assessing the effects of movement-induced changed in cerebral blood volume and consequent filtering of fluorescence, were performed in Thy1-GFP-M mice (n=2; Jax #007788).

2.2. Surgical procedures

2.2.1. Sterile surgery and animal preparation—A sterile field was created by placing a surgical drape over the previously cleaned surgical table, and surgical instruments were sterilized with a hot bead sterilizer for 20s (Fine Science Tools; Model 18000-45). Mice were anesthetized with isoflurane (2% induction, 1.5% maintenance in air) and then mounted in a stereotactic frame in with the skull level between lambda and bregma (Figure 1A). The eyes were treated with eye lubricant (Lacrilube; www.well.ca) to keep the cornea moist, and body temperature was maintained at 37°C using a feedback-regulated heating pad monitored by a rectal probe. Lidocaine (0.1 ml, 0.2%) was injected under the scalp, and mice also received a 0.5 ml subcutaneous injection of a saline solution containing burprenorphine (2 mg/ml), atropine (3μg/ml), and glucose (20mM). The fur on the head of the mouse (from cerebellar plate to near the eyes) was removed using a fine battery powered beard trimmer, and the skin was prepared with a triple scrub of 0.1% Betadine in water followed by 70% ethanol (Figure 1B). Respiration rate and response to toe pinch was checked every 10–15 min to maintain surgical anesthetic plane.

2.2.2. Chronic through-bone window implant—Prior to starting the surgery, a No. 1 circular cover-glass (Marienfeld, Lauda-Konigshofen, Germany; Cat#:0111520) was cut with a diamond pen (ThorLabs, Newton, NJ, USA; Cat#: S90W) to the size of the final cranial window (~9 mm diameter, Fig 1). A skin flap extending over both hemispheres approximately 8 mm in diameter (3 mm anterior to bregma to posterior end of skull and down lateral to eye level) was cut and removed (Figure 1C). A #10 scalpel (curved) and sterile cotton tips were used to gently wipe off any fascia or connective tissue on the skull surface making sure it was completely clear of debris and dry before proceeding. The clear version of C&B-Metabond (Parkell, Edgewood, NY, USA; Product: C&B Metabond) dental cement was prepared by mixing 1 scoop of C&B Metabond powder (Product: S399), 6 drops of C&B Metabond Quick Base (Product: S398) and one drop of C&B Universal catalyst (Product: S371) in a ceramic or glass dish (do not use plastic). Once the mixture reaches a consistency that makes it stick to the end of a wooden stir stick, a head-fixing screw was glued to the cerebellar plate by applying a small amount of dental cement to the butt end of a 4/40 stainless steel setscrew and holding it pressed against the skull until the cement partially dried (1–2 min; Figure 1D). The screw was slightly angled posteriorly (~120° relative to skull) and was centered directly posterior of lambda. With the set-screw in place, a layer of dental adhesive was applied directly on the intact skull (Figure 1E). The pre-cut cover glass was gently placed on top of the mixture before it solidifies (within 1 min) taking care to avoid bubble formation (Figure 1F). If necessary, extra dental cement was applied around the edge of the cover slip to ensure that all of the exposed bone was covered (Figure 1G), and that the incision site was sealed at the edges. The skin naturally tightens itself around the craniotomy and sutures are not necessary. The mixture remains transparent after it solidifies and one should be able to clearly see large surface veins and arteries at the end of the procedure.

2.2.3. Recovery and post-operative monitoring—Once the dental cement around the coverslip is completely solidified (up to 20 min), the animal received a second SC injection of saline (0.5 ml) with 20 mM of glucose, and allowed to recover in the home cage with an over-head heat lamp and intermittent monitoring (hourly for the first 4 h and every 4–8h thereafter for activity level).

2.3. Chronic wide-field imaging in awake mice

We generally wait 7 days after chronic window implantation before performing head-fixed imaging to provide sufficient time for the incision to heal. The headfixing apparatus was constructed by attaching a locking ball and socket mount (Thorlabs, Product: TRB1) to an aluminum base plate using two optical posts and a 90° turn (Figure 2A, B). To couple the head-fixing screw on the mouse (4/40 threads) to the ball and socket mount (8/32 threads), an ER025 post (Thorlabs) was modified by re-tapping one end of it with 8/32 threads to fit the ball and socket mount. A clear Plexiglas tube (28mm diameter), was attached to the base plate to provide a snug chamber for the mouse to rest during imaging sessions.

Following 2–3 sessions (5 min each) of handling and habituation to the Plexiglas tube, mice can be gently coaxed into the fixation tube without anesthesia, which eliminates anesthetic side-effects such as a drop in body temperature (Sessler, 2000) and decreased cortical activity (Greenberg et al., 2008). For head fixation, the set-screw on the head of the mouse was fitted with a nut, and threaded into the ER025 post by rotating the ball within the socket. The nut was then tightened upward against the ER025 post to immobilize the head, without applying any torque or pressure on the cranial window. The articulating ball and socket allowed us to make fine adjustments to head position to increase the comfort of the animals, and to align the chronic window under the camera. Once the desired position was achieved, all joints were carefully tightened to eliminate movement.

Head fixed mice were placed under a macroscope made from a pair of back-to-back video lenses (50 mm, 1.4 f:135 mm, 2.8 f or 50 mm, 1.4 f:30 mm, 2 f; Figure 2C). The cranial window was illuminated with blue light emitting diodes (LED; Luxeon, 470 nm), constructed by placing a 470/20 nm band-pass filter (Chroma, Product: ET470/20x) and a 25.4 mm bi-convex lens (Thorlabs, Product: LB1761) in front of the LED (25.4 mm from LED) to shape the beam to the approximate size of the cranial window (Figure 2D). This allowed us to restrict illumination to the cranial window, while avoiding the eyes and also ensured relatively homogeneous illumination across the cortex (see Figure 3C). Fluorescence GCaMP signal was collected through a 525/36nm (Chroma, Product: ET525/36m) band-pass filter and captured with a 1M60 Pantera CCD camera (Dalsa). In order to reduce file size and minimize the power of excitation light used, we typically bin camera pixels (8×8) thus producing a resolution of 68μm/pixel. These imaging parameters have been used previously for voltage sensitive dye imaging (Mohajerani et al., 2013) as well as anesthetized GCaMP3 imaging of spontaneous activity in mouse cortex (Vanni and Murphy, 2014). The activity of the mouse during imaging sessions was monitored with a webcam that was modified by removing the IR filter from the lens assembly, attaching a 590 nm long-pass filter (Thorlabs, Product: FGL590) in front of the lens, and illuminating the mouse with an IR LED (850nm, Figure 2C). Some bandpass filters also pass higher

wavelength IR light, therefore we also added an IR filter (720±25nm; Thorlabs, Product FM01) on top of our emission filter to avoid contaminating the GCaMP signal with the IR illumination. For spontaneous activity analysis we collected 12-bit images at 30 Hz for 5 min (total of 9,000 frames) using XCAP imaging software (EPIX Inc., Buffalo Grove IL). A custom written Matlab (Mathworks) script (see appendix) was used to create correlation maps and matrixes using previously published methods (Vanni and Murphy, 2014). Importantly, all analyses were carried out on ΔF/F values to correct for slight differences in baseline fluorescence intensity resulting from the curvature of the brain along the lateral edges and at midline.

In order to directly compare our awake spontaneous activity recordings to anesthetised recordings in a subset of animals (n=2) we attached a small anaesthesia mask to the headfixing assembly and anesthetised mice with 1.3% isofluorane for a second 5-min recording (immediately after the awake recording).

The stability of the cranial window was assessed by quantifying both vertical and lateral movement using two laser motion sensors (Keyence, Osaka, Japan; Model: LK-2000). One was targeted to the anterior portion of the cranial window to measure vertical movement, and the second was pointed at the side of the cranial window (in line with bregma) to assess lateral movement.

The optical transparency of the preparation was quantified by measuring the contrast values at vessel borders. Loss of optical transparency would increase light scattering and thus add blurring artefacts to images, resulting in decreased contrast values. To address the resolution of our preparation, we measured the point spread function (SPF) using 10μm latex beads (Polysciences Inc., Cat. # 18140-2) that were attached to the intracranial bone surface of our chronic window preparation. This was achieved by carefully removing the chronic window from a euthanized mouse such that the skull remained attached to the dental cement/coverglass assembly. We then applied microspheres to the under side of the bone, and maintained the preparation moist while we imaged the beads through the chronic window.

3. RESULTS

The surgical preparation we describe is simple to perform even for relatively inexperienced surgeons (takes ~30 minutes), as the skull is maintained intact. The chance for inadvertent brain damage is minimal as the only manipulation to the skull is the gentle clearing of connective tissue with cotton tips and a scalpel once the scalp is removed. In our laboratory we have prepared ~120 animals using this procedure and we have had no cases of mortality or early euthanasia due to surgical complications. In addition, we did not experience any head-cap detachments during imaging (n=13 mice), however when windows were maintained beyond the 2-month period of the current experiment, window quality deteriorated in a subset of mice (30–40%) due to growth of connective tissue on top of the skull and the bone becoming opaque (data not shown). In addition to simplicity, another advantage of our method is that animals can be group housed, as the stainless steel head attachment screw cannot be chewed by cage mates, nor is it protruding enough to produce inadvertent damage to other mice in the cage or catch in wire top bars.

The size and position of the cranial window can be modified slightly to meet experimental needs. Our windows were approximately 11 mm (A-P) by 9 mm (M-L), covering the cortical area between the anterior sinus and lambda. Previous studies have performed imaging over a similar spatial scale in acute preparations by continuously moistening the skull with saline (Kalchenko et al., 2014). We compared the optical access provided by our chronic preparation to the acute saline soaked skull and found that using identical imaging parameters (LED excitation light = 0.36mW/mm^2, exposure = 1s, 1024×1024 pixels) produced comparable fluorescence images between the two preparations (Figure 3A). These findings indicate that the dental cement does not introduce gross optical aberrations, but instead maintains the skull semi-transparent, as when moist with aqueous solution. Our assessment of the PSF (Figure 3B) while imaging through the chronic window preparation (including skull) indicates that sub-resolution microspheres (10μm) appear to be 48.63±5.7μm in diameter, which is still smaller than the pixel size (68μm) during widefield imaging.

We found that within imaging sessions the intensity of the fluorescence signal was stable across our 5-minute recordings, with only 2.7±0.65% bleaching of the raw signal (n=7; Figure 3C). We assessed the homogeneity of the fluorescence signal across the imaging window by comparing the intensity of a row of pixels across a chronic window with the signal from a fluorescent slide (Figure 3D). The curvature of the brain at midline and the lateral edges diminished the amount of fluorescence signal, however all data analysis was performed on data normalized by baseline fluorescence (ΔF/F).

We assessed both vertical and lateral brain movement during awake imaging using laser motion sensors targeted at the cranial window (Figure 4A). These measurements showed that the largest movements occurred while the animal was engaged in grooming (maximum lateral movement = 25.1±11.84μm; maximum vertical movement = 14.8±3.2μm; n=4 mice), while the average movement was 6.9±4.3μm lateral and 1.9±0.5μm vertical. These shifts were much smaller than a single pixel (68μm; Figure 4B, C) or the ~300 μm focal volume of our macroscope (Ratzlaff and Grinvald, 1991). To further confirm these measurements, lateral brain movement was also evaluated using the images of the surface vasculature as landmarks. A custom written Matlab script was used to calculate the spatial cross-correlation for each shift (ΔX, ΔY) of each frame, relative to the average time projection of all frames. For each frame, the highest correlation value was used to determine the optimal shift and the largest shift: $\sqrt{\Delta X^2+\Delta Y^2}$. These measurements confirmed that even during bouts of limb and body movements, the largest shifts in brain position were sub-pixel in size (average maximum movement = 22μm, n=7 mice; Figure 4D). Based on these results we conclude that it is not necessary to implement movement-correction algorithms during our analyses of wide-field calcium imaging.

To determine whether this preparation is suitable for awake imaging of spontaneous activity (Mohajerani et al., 2013), we generated seed-pixel correlation maps using methods similar to anesthetized preparations (Vanni and Murphy, 2014). In control experiments we assessed the contribution of movement-induced blood volume artefacts by recording fluorescence signal from awake Thy1-GFP-M mice using the same imaging parameters as GCaMP imaging (Figure 5). We found that after filtering the GFP signal at 1–10Hz, we could not reveal any

correlations either within or between hemispheres that were similar in magnitude to those present in GCaMP mice. In contrast, applying this filter band to GCaMP signal maintained strong intra- and inter-hemispheric correlations. Therefore we chose to perform all analyses of GCaMP signals using the 1–10Hz frequency band. Seed pixels were placed in 3 different cortical regions (Figure 6A, B; barrel cortex, hind-limb sensorimotor cortex, primary motor cortex), and we found the most consistent correlated activity with the contralateral (homotopic) cortex, while the strongest intra-hemispheric correlation was between the barrel and vibrissae motor cortex (Figure 6C). Importantly, both the spatial pattern of these motifs as well as the relative strength of the correlation values was similar between awake and anesthetized states (Figure 6C, D), suggesting that any potential artifacts induced by mouse movement were either removed through our filtering procedure, or do not contribute to the structure of correlation maps. Our results confirm that our through-bone, awake imaging preparation provides sufficient optical access to identify functional motifs in sensory and association cortical regions through seed pixel correlation analysis in awake mice.

For longitudinal studies we typically perform intermittent imaging in awake mice for up to 2 months. Chronic windows remain clear and stable for this duration, with surface vasculature clearly visible, and correlation maps showing similar structure across imaging sessions (Figure 7A). We assessed optical clarity of our windows by measuring the contrast values of individual vessels over 8 weeks (Figure 7B). Window deterioration would be expected to create blurring artefacts and thus decrease contrast values of the same vessel over time. However, our results show that contrast values remained stable for 8 weeks, with little apparent deterioration of window quality (Figure 7C). In addition we did not have to increase excitation light power (0.36mW/mm^2) or camera exposure (30ms) to achieve a constant level of fluorescence (~3000 grey levels) across the imaging sessions, suggesting that both optical transparency and GCaMP6 expression in the cortex are stable over the long-term.

4. DISCUSSION

We describe here our procedures for generating a chronic window that allows us to perform, bi-hemispheric wide-field imaging in awake GCaMP6 transgenic mice. Our preparation has several advantages over other cranial widows. First, the surgical procedure is fast and simple to preform, with little risk for inadvertent damage or inflammation that can occur during bone thinning or craniotomy procedures (Xu et al., 2007; Yang et al., 2009). Second, the large imaging area extending over both hemispheres facilitates the investigation of multiple regions of interest within the same animal, or the tracking of experimentally-induced shifts in functional maps. For example, the effects of unilateral manipulations such as focal ischemia may be evaluated by quantifying neuronal activity in regions distal from the stroke (such as the intact hemisphere) as well as a number of peri-infarct regions in the stroke hemisphere. A third advantage of our method is that the simple headfixing screw facilitates immobilization without the use of anesthetics, which may inhibit cortical activity (Greenberg et al., 2008), and also limits the frequency of imaging sessions that can be performed for each animal. Some behavioural training paradigms require multiple head-fixed training sessions per day over several weeks (Chen et al., 2015), which would not be feasible should the mice need to be anesthetized for each training session. Alternative head-

fixation devices utilizing ring-shaped chambers offer greater stability and may be used for cellular-level two-photon microscopy, however the larger footprint of the ring attachment reduces the imaging area (Hefendehl et al., 2012; Osborne and Dudman, 2014). In addition to the Metabond adhesive used here and in other studies (Hira et al., 2009), chronic windows may also be created with clear-drying OrthoJet adhesive (Guo et al., 2015) or with cyanoacrylate based adhesives (Yang et al., 2010). Although we anticipate there to be slight differences between materials (such as drying time during surgery), all three of these adhesives have been used for some form transcranial imaging or optogenetic stimulation in mice (Drew et al., 2010; Hilton et al., 2016; Silasi et al., 2013; Vanni and Murphy, 2014; Yang et al., 2010).

The preparation we describe here evolved from previous work where the skull thinning technique originally developed for two-photon imaging (Drew et al., 2010; Yoder and Kleinfeld, 2002) was expanded to create a bilateral preparation to facilitate optogenetic stimulation in both hemispheres (Silasi et al., 2013). In contrast to full craniectomies, where a piece of the skull is removed (Ricardo and Carlos, 2008), skull-thinning preparations are less invasive, reducing inflammation and gliosis (Xu et al., 2007). However, for mesoscopic wide-field imaging, where cellular resolution is not the goal, we wanted to reduce the invasiveness even further by keeping the skull completely intact for chronic imaging. We were motivated by experiments performing through-bone imaging of intrinsic signals in anesthetized mice (White et al., 2011), which are much smaller in amplitude than the GCaMP6 signal. Indeed, we have successfully used our preparation to also generate sensory maps in anesthetized animals using intrinsic imaging (Vanni and Murphy, 2014).

In addition to wide-field imaging, there is also great interest in performing cellular resolution, two-photon imaging through intact bone preparations (Yoder and Kleinfeld, 2002). A recent study demonstrated that advanced wavefront correction can compensate for high-order aberrations in the mouse skull, thus making it possible to resolve structures on the micron scale within the mouse brain (Park et al., 2015). Although we have not attempted two-photon imaging through our preparation, relatively minor additions to two-photon imaging hardware (a MEMS deformable mirror) may in the future make such experiments feasible. The possibility of combining wide-field mesoscopic imaging with cellular resolution 2-photon imaging of neuronal activity, or performing targeted laser ablation (Murakami et al., 2015) within the same subjects may facilitate studies that were not previously possible with standard craniotomy procedures. Our preparation may also be adapted for other imaging tools that can be performed trans-cranially, such as optical coherence tomography (OCT) (Cang et al., 2005). Newly optimized algorithms and scanning protocols can provide quantitative measurements of cerebral blood flow with OCT in rodents (Yang et al., 2010), therefore opening the possibility for performing longitudinal measures of flow in disease models such as stroke or dementia.

We demonstrate the utility of our preparation by performing wide-field imaging of neuronal activity in awake mice and examine functional connectivity through seed pixel correlation analyses. Such analyses have been previously performed in anesthetized preparations (Vanni and Murphy, 2014), however this is the first demonstration that similar correlation maps emerge from spontaneous activity in awake mice. Neuronal activity was measured in

GCaMP6 transgenic mice (Madisen et al., 2015), which produce a delta F response approximately 10x larger than GCaMP3 transgenic mice (Murakami et al., 2015), and also require slightly lower excitation light (GCaMP3 = 0.5mW/mm^2 (Vanni and Murphy, 2014). vs. GCaMP6 = 0.36mW/mm^2) to achieve a similar level of resting fluorescence. Both of these effects are likely due to the substantial improvement in the expression system provided by the Cre/tTA driver, relative to the Rosa-CAG reporters used for GCaMP3 (Madisen et al., 2015). Because intracellular calcium levels are related to the change of spiking activity at the cellular scale (Stosiek et al., 2003; Tian et al., 2009), a wide-field fluorescence response (that is targeted to neurons) serves as reliable indicator of neuronal activity. The use of transgenic mice represents an opportunity to map neuronal activity over large regions without the need to perform virus injections or dye loading. In addition, the consistent and stable level of expression between animals makes it possible to average data from multiple mice. The development of through-bone chronic imaging windows that provides optical access to the majority of the dorsal cortical surface has made this a relatively simple and noninvasive procedure.

Acknowledgments

This work was supported by Canadian Institutes of Health Research (CIHR) Operating Grant MOP-12675 to T.H.M., a CIHR fellowship to G.S. and Michael Smith Foundation for Health Research postdoctoral fellowship to M.P.V. T.H.M. and G.S. are supported by the Canadian Partnership for Stroke Recovery. We thank Pumin Wang for surgical assistance and Jeff LeDue for assistance with optics.

References

Aravanis AM, Wang L-PP, Zhang F, Meltzer LA, Mogri MZ, Schneider MB, Deisseroth K. An optical neural interface: in vivo control of rodent motor cortex with integrated fiberoptic and optogenetic technology. Journal of neural engineering. 2007; 4:56.

Cang J, Kalatsky VA, LÖwel S, Stryker MP. Optical imaging of the intrinsic signal as a measure of cortical plasticity in the mouse. Visual neuroscience. 2005; 22:685–91. [PubMed: 16332279]

Chen JL, Margolis DJ, Stankov A, Sumanovski LT, Schneider BL, Helmchen F. Pathway-specific reorganization of projection neurons in somatosensory cortex during learning. Nature Neuroscience. 2015

Dombeck DA, Khabbaz AN, Collman F, Adelman TL, Tank DW. Imaging large-scale neural activity with cellular resolution in awake, mobile mice. Neuron. 2007; 56:43–57. [PubMed: 17920014]

Drew PJ, Shih AY, Driscoll JD, Knutsen PM, Blinder P, Davalos D, Akassoglou K, Tsai PS, Kleinfeld D. Chronic optical access through a polished and reinforced thinned skull. Nature methods. 2010; 7:981–4. [PubMed: 20966916]

Emiliani V, Cohen AE, Deisseroth K, Häusser M. All-Optical Interrogation of Neural Circuits. The Journal of neuroscience : the official journal of the Society for Neuroscience. 2015; 35:13917–26. [PubMed: 26468193]

Gaffield MA, Amat SB, Bito H, Christie JM. Chronic imaging of movement-related Purkinje cell calcium activity in awake behaving mice. Journal of neurophysiology. 2015

Greenberg DS, Houweling AR, Kerr JND. Population imaging of ongoing neuronal activity in the visual cortex of awake rats. Nature Neuroscience. 2008:11. [PubMed: 18073776]

Guo J-ZZ, Graves AR, Guo WW, Zheng J, Lee A, Rodríguez-González J, Li N, Macklin JJ, Phillips JW, Mensh BD, Branson K, Hantman AW. Cortex commands the performance of skilled movement. eLife. 2015:4.

Guo ZV, Li N, Huber D, Ophir E, Gutnisky D, Ting JT, Feng G, Svoboda K. Flow of cortical activity underlying a tactile decision in mice. Neuron. 2014; 81:179–94. [PubMed: 24361077]

Hefendehl JK, Milford D, Eicke D, Wegenast-Braun BM, Calhoun ME, Grathwohl SA, Jucker M, Liebig C. Repeatable target localization for long-term in vivo imaging of mice with 2-photon microscopy. Journal of neuroscience methods. 2012; 205:357–63. [PubMed: 22093765]

Hilton BJ, Anenberg E, Harrison TC, Boyd JD, Murphy TH, Tetzlaff W. Re-Establishment of Cortical Motor Output Maps and Spontaneous Functional Recovery via Spared Dorsolaterally Projecting Corticospinal Neurons after Dorsal Column Spinal Cord Injury in Adult Mice. Journal of Neuroscience. 2016; 36:4080–92. [PubMed: 27053214]

Hira R, Honkura N, Noguchi J, Maruyama Y, Augustine GJ, Kasai H, Matsuzaki M. Transcranial optogenetic stimulation for functional mapping of the motor cortex. Journal of neuroscience methods. 2009; 179:258–63. [PubMed: 19428535]

Hira R, Terada SI, Kondo M, Matsuzaki M. Distinct Functional Modules for Discrete and Rhythmic Forelimb Movements in the Mouse Motor Cortex. Journal of Neuroscience. 2015; 35:13311–22. [PubMed: 26424880]

Holtmaat A, Bonhoeffer T, Chow DK, Chuckowree J, De Paola V, Hofer SB, Hübener M, Keck T, Knott G, Lee W-CAC, Mostany R, Mrsic-Flogel TD, Nedivi E, Portera-Cailliau C, Svoboda K, Trachtenberg JT, Wilbrecht L. Long-term, high-resolution imaging in the mouse neocortex through a chronic cranial window. Nature protocols. 2009; 4:1128–44. [PubMed: 19617885]

Jennings JH, Ung RL, Resendez SL, Stamatakis AM, Taylor JG, Huang J, Veleta K, Kantak PA, Aita M, Shilling-Scrivo K, Ramakrishnan C, Deisseroth K, Otte S, Stuber GD. Visualizing Hypothalamic Network Dynamics for Appetitive and Consummatory Behaviors. Cell. 2015:160.

Kalchenko V, Israeli D, Kuznetsov Y, Harmelin A. Transcranial optical vascular imaging (TOVI) of cortical hemodynamics in mouse brain. Scientific Reports. 2014

Kalmbach AS, Waters J. Brain surface temperature under a craniotomy. Journal of neurophysiology. 2012; 108:3138–46. [PubMed: 22972953]

Madisen L, Garner AR, Shimaoka D, Chuong AS, Klapoetke NC, Li L, Bourg A, Niino Y, Egolf L, Monetti C. Transgenic mice for intersectional targeting of neural sensors and effectors with high specificity and performance. Neuron. 2015; 85:942–58. [PubMed: 25741722]

Madisen L, Mao T, Koch H, Zhuo J-mM, Berenyi A, Fujisawa S, Hsu Y-WAW, Garcia AJ, Gu X, Zanella S, Kidney J, Gu H, Mao Y, Hooks BM, Boyden ES, Buzsáki G, Ramirez JM, Jones AR, Svoboda K, Han X, Turner EE, Zeng H. A toolbox of Cre-dependent optogenetic transgenic mice for light-induced activation and silencing. Nature neuroscience. 2012; 15:793–802. [PubMed: 22446880]

Mohajerani MH, Chan AW, Mohsenvand M, LeDue J, Liu R, McVea DA, Boyd JD, Wang YT, Reimers M, Murphy TH. Spontaneous cortical activity alternates between motifs defined by regional axonal projections. Nature neuroscience. 2013; 16:1426–35. [PubMed: 23974708]

Murakami T, Yoshida T, Matsui T, Ohki K. Wide-field Ca2+ imaging reveals visually evoked activity in the retrosplenial area. Frontiers in Molecular Neuroscience. 2015:08.

Oh SW, Harris JA, Ng L, Winslow B, Cain N, Mihalas S, Wang Q, Lau C, Kuan L, Henry AM, Mortrud MT, Ouellette B, Nguyen TN, Sorensen SA, Slaughterbeck CR, Wakeman W, Li Y, Feng D, Ho A, Nicholas E, Hirokawa KE, Bohn P, Joines KM, Peng H, Hawrylycz MJ, Phillips JW, Hohmann JG, Wohnoutka P, Gerfen CR, Koch C, Bernard A, Dang C, Jones AR, Zeng H. A mesoscale connectome of the mouse brain. Nature. 2014; 508:207–14. [PubMed: 24695228]

Osborne JE, Dudman JT. RIVETS: a mechanical system for in vivo and in vitro electrophysiology and imaging. PloS one. 2014:9.

Park J-H, Sun W, Cui M. High-resolution in vivo imaging of mouse brain through the intact skull. Proceedings of the National Academy of Sciences. 2015:112.

Ratzlaff EH, Grinvald A. A tandem-lens epifluorescence macroscope: hundred-fold brightness advantage for wide-field imaging. Journal of neuroscience methods. 1991; 36:127–37. [PubMed: 1905769]

Ricardo M, Carlos PC. A craniotomy surgery procedure for chronic brain imaging. Journal of Visualized Experiments. 2008

Sessler DI. Perioperative heat balance. Anesthesiology. 2000; 92:578–96. [PubMed: 10691247]

Silasi G, Boyd JD, Ledue J, Murphy TH. Improved methods for chronic light-based motor mapping in mice: automated movement tracking with accelerometers, and chronic EEG recording in a bilateral thin-skull preparation. Frontiers in neural circuits. 2013; 7:123. [PubMed: 23966910]

Silasi G, Murphy TH. Stroke and the Connectome: How Connectivity Guides Therapeutic Intervention. Neuron. 2014:83.

Stosiek C, Garaschuk O, Holthoff K, Konnerth A. In vivo two-photon calcium imaging of neuronal networks. Proceedings of the National Academy of Sciences of the United States of America. 2003; 100:7319–24. [PubMed: 12777621]

Tian L, Hires SA, Mao T, Huber D, Chiappe ME, Chalasani SH, Petreanu L, Akerboom J, McKinney SA, Schreiter ER, Bargmann CI, Jayaraman V, Svoboda K, Looger LL. Imaging neural activity in worms, flies and mice with improved GCaMP calcium indicators. Nature methods. 2009; 6:875–81. [PubMed: 19898485]

Vanni MP, Murphy TH. Mesoscale Transcranial Spontaneous Activity Mapping in GCaMP3 Transgenic Mice Reveals Extensive Reciprocal Connections between Areas of Somatomotor Cortex. Journal of Neuroscience. 2014

White BR, Bauer AQ, Snyder AZ, Schlaggar BL, Lee J-MM, Culver JP. Imaging of functional connectivity in the mouse brain. PloS one. 2011:6.

Xu H-TT, Pan F, Yang G, Gan W-BB. Choice of cranial window type for in vivo imaging affects dendritic spine turnover in the cortex. Nature neuroscience. 2007; 10:549–51. [PubMed: 17417634]

Yang G, Pan F, Gan W-BB. Stably maintained dendritic spines are associated with lifelong memories. Nature. 2009; 462:920–4. [PubMed: 19946265]

Yang G, Pan F, Parkhurst CN, Grutzendler J, Gan W-BB. Thinned-skull cranial window technique for long-term imaging of the cortex in live mice. Nature protocols. 2010; 5:201–8. [PubMed: 20134419]

Yoder EJ, Kleinfeld D. Cortical imaging through the intact mouse skull using two-photon excitation laser scanning microscopy. Microscopy Research and Technique. 2002:56.

Appendix 1. MATLAB script for generating seed pixel correlation maps and matrixes

```
%% 1. Open data
clear all, clc
[file,rep] = uigetfile([pwd '*.*']); % select file
SF = input('Sampling Frequency (Hz): '); % set sampling
file = [rep file];
info = imfinfo(file); % open file info
F = length(info); % number of frame
I = zeros(info(1).Width,info(1).Height,F,'uint16'); % data
matrix
for i = 1:F, I(:,:,i) = imread(file,'Index',i,'Info',info);
end; % reading
I = reshape(single(I),size(I,1)*size(I,2),size(I,3));
TT = squeeze(mean(I,1)); TT = TT / mean(TT); % global activity
C = zeros(size(I),'single'); % correction matrix
MMM = imresize(mean(I,2),[size(I,1) size(I,2)]);
TTT = imresize(TT,[size(I,1) size(I,2)]);
I = I - (MMM.*TTT); % substraction of the normalized global
```

```
activity
[b,a] = cheby1(2,0.5,2*[1 10]/SF); % band pass (1 to 10Hz)
filtering
for i = 1:size(I,1), I(i,:) =
single(filtfilt(b,a,double(I(i,:)))); end
%% 2. Seed pixel correlation
CM = zeros(info(1).Width,info(1).Height,'single'); %
correlation matrix
for i = 1:1000
     imshow(CM,[-1 1]), colormap jet, colorbar,
     try, hold on, plot(x,y,'wo'); hold off, end
     [x,y]=ginput(1); x = round(x); y = round(y); % select a
pixel
     CM = corr(squeeze(I((x-1)*info(1).Width+y,:))',I'); %
pixelwise correlation
     CM = reshape(CM,info(1).Width,info(1).Height);
end;
```

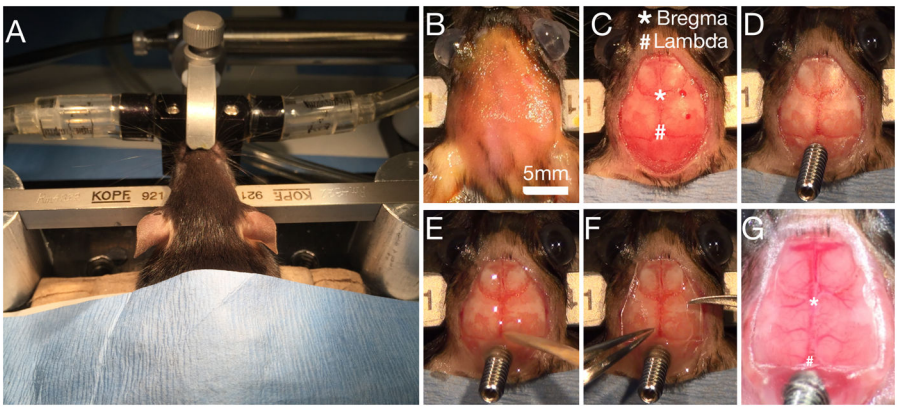

Figure 1. Surgical procedure for chronic window implant

Anesthetized mice are stabilized in a stereotaxic frame (A), the skin between the ears and eyes is shaved (B) and the skin covering the occipital, parietal and frontal bones is cut away (C). The underlying skull is cleared of fascia and a setscrew is attached with dental cement over the occipital bone (D). A thick layer of dental cement is applied over the exposed (intact) skull (E) and a piece of coverglass is carefully lowered over the cement (F). In contrast to the opaque nature of the dry skull (C, D), once the chronic preparation dries, surface vessels are clearly visible through the intact skull (G).

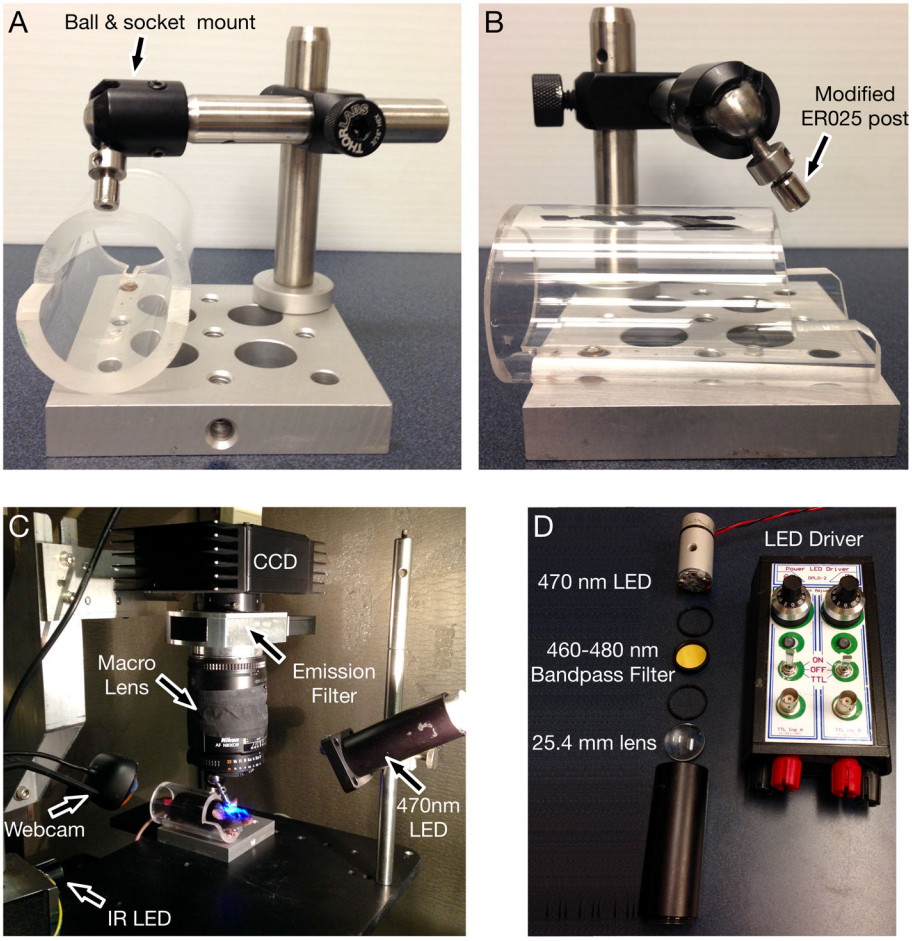

Figure 2. Hardware for head-fixation, and awake wide-field calcium imaging

The head-fixing screw surgically implanted into the chronic window is attached to a ball and socket articulating joint (A) trough a modified ER025 post (B). The mice are coaxed into the Plexiglas body chamber, headfixed, and placed under the imaging system while fully awake. Imaging is performed in a darkened, sound-proof chamber and the mice are monitored via a webcam with IR illumination (C). The excitation light for GCaMP imaging is constructed by assembling a 470 nm LED, a bandpass filter and focusing lens within an aluminum tube. An LED driver is used to provide stable DC voltage to the LED (D).

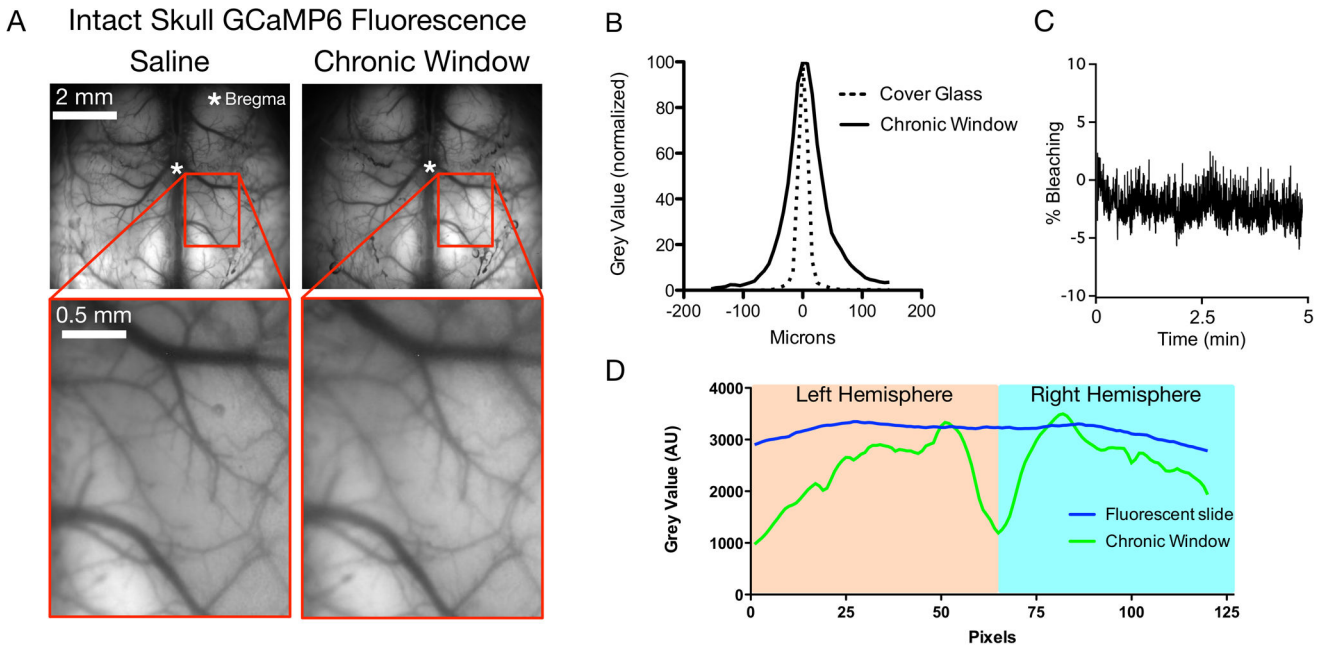

Figure 3. Chronic window preparation maintains skull transparency as when moist with aqueous solution

When moistened with saline, the mouse skull becomes adequately transparent to clearly see surface vasculature in fluorescence images (A, left). Our cranial window preparation maintains a similar level of transparency (A, right). We imaged sub-resolution fluorescent beads (10μm diameter) either through a cover glass (control) or through the chronic window preparation to derive a point spread function for our imaging system (B). This preparation facilitates stable recording of GCaMP6 signal over several minutes without significant photobleaching (2.7% relative to first frame, n=7 mice; C). Due to the curvature of the skull at the lateral edges as well as filtering effects of the superior sagittal sinus (midline) the intensity of fluorescence signal is not homogeneous across the cortex. For this reason, all analyses were performed on ΔF/F values, thus correcting for slight differences in baseline fluorescence.

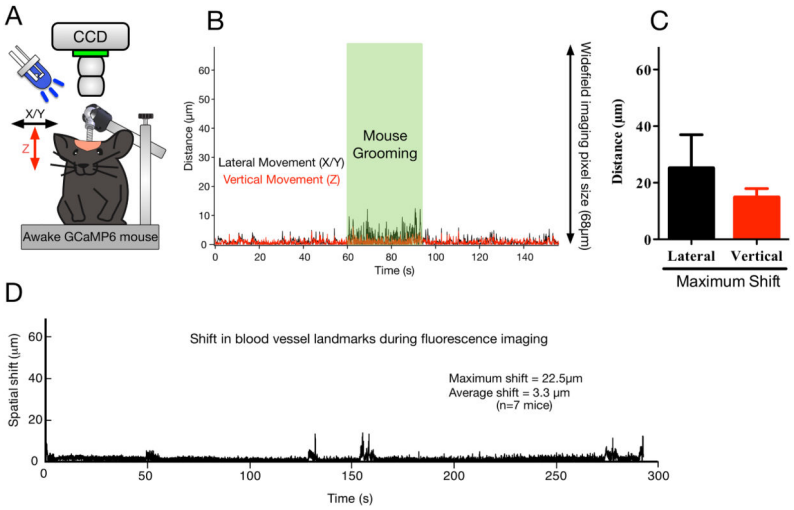

Figure 4. Assessment of brain movement during awake imaging

Laser position sensors targeted to the top and side of the cranial window were used to measure vertical and lateral movement respectively in an awake mouse (A). The largest movements (~13μm) occurred while the mouse was engaged in grooming, while quiescent periods were associated with less than 10 μm movements (B). Group average (n=4) for largest vertical and lateral movements are smaller than the pixel size in our imaging setup (C). Shifts in surface vasculature during fluorescence imaging were also used to quantify the amount of horizontal movement during awake imaging. The largest movements were observed during bouts of body and limb movements, and were on average 22.5 μm in amplitude (n=7 mice; D).

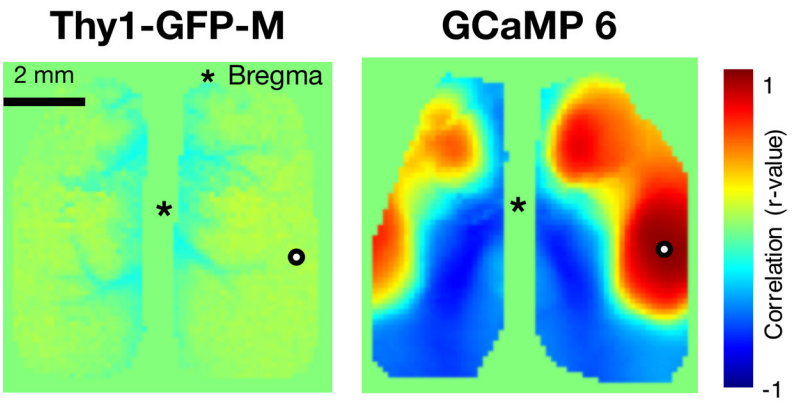

Figure 5. Lack of intra- and inter-hemispheric correlations during awake imaging of Thy1-GFP-M mice

Mice expressing GFP in cortical cells were used to examine if movement induced blood volume changes may contribute to the structure of seed-pixel correlation maps. We found that filtering data at 1–10Hz eliminated most intra- and inter-hemispheric correlations in spontaneous activity recordings from GFP mice, while strong correlations were maintained in GCaMP mice. White circle indicates location of seed pixel in right hemisphere.

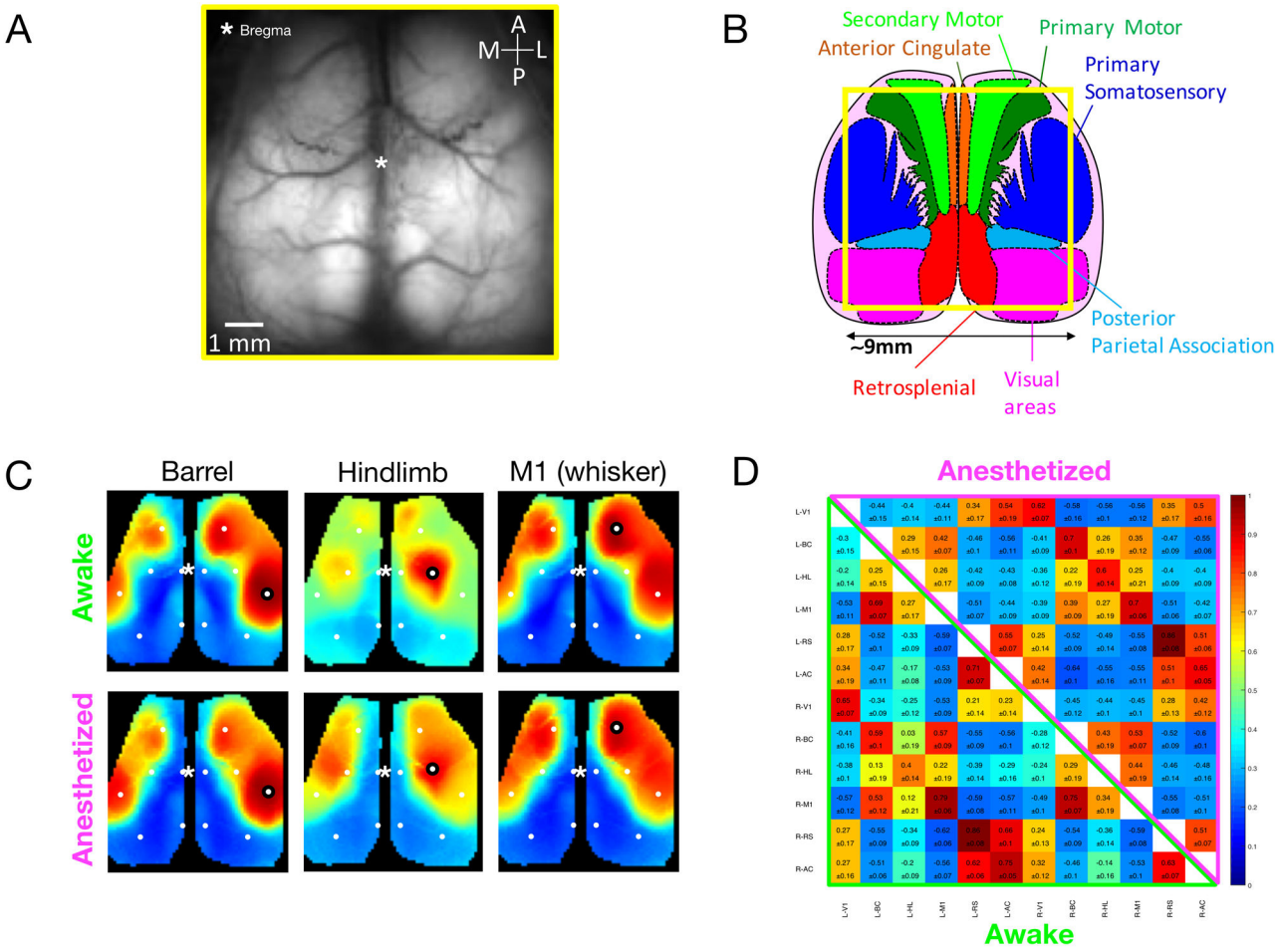

Figure 6. Seed-pixel correlation maps and matrixes in awake and anesthetized mice

Our cranial window preparation (A) allows us to image activity in multiple primary sensory, motor as well as association areas (B). Seed-pixel correlation maps reveal cortical motifs that are similar between awake (C, upper) and anesthetized (C, lower) states (Isoflurane). The group averages for correlation values in awake (n=7) and anesthetized (n=2) mice were similar between the two states, with the homotopic cortex showing the most reliable correlated activity (D).

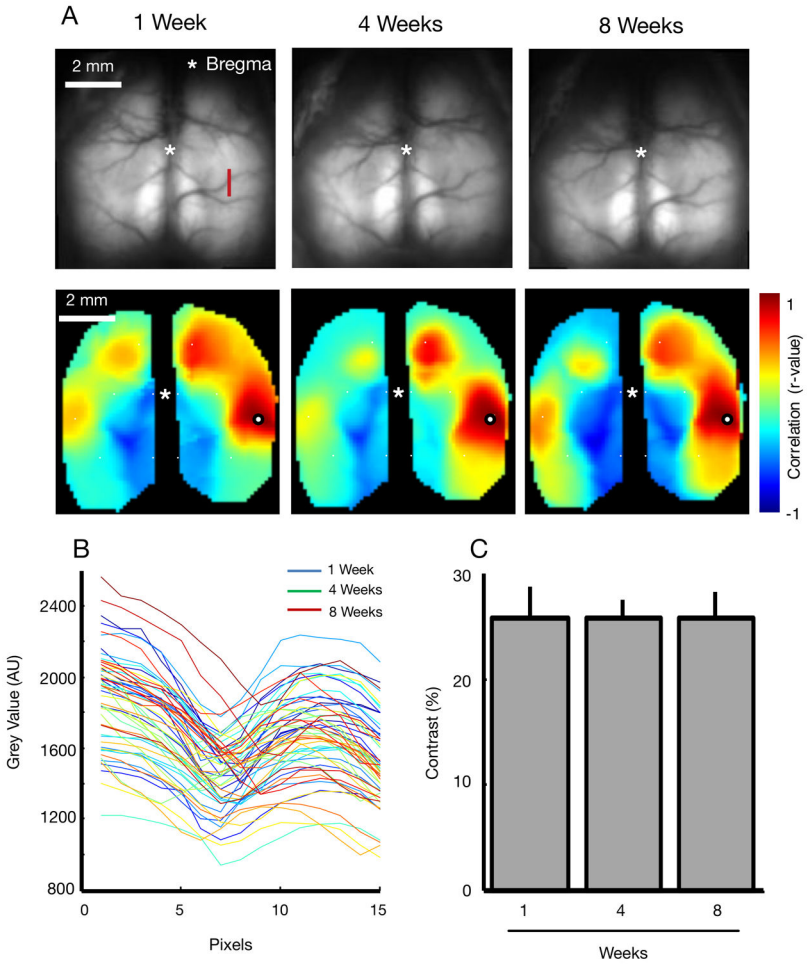

Figure 7. Transcranial windows maintain optical transparency for at least 8 weeks

Surface vasculature remained clearly visible, and spontaneous activity recordings showed similar correlation maps for at least 8 weeks after chronic window implantation (A). Line plots of contrast values for vessel over 8 weeks (B). An example vessel included in the analysis is indicated by red line in (A) Group analysis showed no significant changes over time (n=3 mice, 30 vessels analyzed), indicating that the quality of the chronic window does not deteriorate (C).